LESZEK JARECKI*), ANDRZEJ ZIABICKI

Institute of Fundamental Technological Research
Polish Academy of Sciences
Polymer Physics Laboratory
ul. Świętokrzyska 21, 00-049 Warszawa, Poland

Viscosity effects in computer modeling of fiber spinning from crystallizing polymer melts

Summary — Role of local viscosity in the dynamics of melt spinning of a polymer crystallizing under tensile stress are investigated using mathematical modeling methods. The viscosity is assumed to be dependent on local temperature and degree of crystallinity along the spinning axis. Role of the polymer viscosity is studied for PET in the range from low to high spinning speeds. Strong effects of stress-induced crystallization on local polymer viscosity, resulting in crosslinking of chain molecules by arising crystallites, lead to limitation of the spinning speed, and a maximum of the take-up speed is predicted. Effects of the spinning-speed affected viscosity are analysed using simplified models of melt spinning and compared with the complete dynamic model. One concludes that the maximum of take-up speed predicted for high spinning speeds is a consequence of strong rheological effects of online oriented crystallization leading to gelation of the spun polymer by crystallites playing a role of physical crosslinks. Temperature effects on polymer viscosity are not responsible for the limitations of the take-up velocity.

Key words: mathematical modeling of melt spinning, fiber spinning from crystallizing polymer melt, molecular orientation, oriented crystallization, viscosity of crystallizing polymer.

Research and development projects on fiber spinning from polymer melts tend to use computer modeling methods combined with experimental investigations. The main attention in the research is paid to structure development in the spinning line and to its control by the process parameters. Mechanical properties of synthetic fibers are directly related to their structure, *i.e.* molecular orientation and crystallinity. Computational methods offer more economic and fast investigation tool. Nevertheless, complexity of melt spinning with online crystallization, involving several interrelated phenomena, requires thorough investigations on modeling of the process.

In this paper we focus on the role of polymer viscosity coupled with online stress-induced crystallization in the modeling of melt spinning. Rheology of the spun polymer melt is affected by thermal conditions along the spinning line, *i.e.* cooling or modifications of the cooling by online zone heating applied before the take-up point. Spinning with high take-up speeds introduces stress-induced crystallization which considerably affects rheology of the spun melt [1, 2], for example in poly(ethylene terephthalate) (PET). The main rheological effect of crystallization is strong reduction in the melt fluidity dominating effects of the crystallization heat and, finally, solidification of the polymer before the glass transition.

In mathematical modeling, the temperature- and crystallinity-dependent viscosity influences the rheological equation coupled with the force and heat balance equations, as well as with kinetic equation of the online stress-induced crystallization [3]. The crystallization introduces strong nonlinearity to the system of spinning equations causing specific problems in the computations.

Interrelation between kinetics of stress-induced crystallization and melt hardening by crystallization leads to ambiguities between the final and initial boundary conditions when solving the initial value problem for the set of spinning equations. The problem manifests in an appearance of a maximum on the plots of the take-up velocity *vs.* initial tension shown in our earlier publication [4]. The ambiguity concerns relation between the filament velocity at the take-up point and the initial tensile

*) To whom all correspondence should be addressed, e-mail: ljarecki@ippt.gov.pl

force in modeling of PET melt spinning with typical cooling, as well as with heating zone. Heating zone, applied next to cooling one in the spinning, modifies crystallization in the spun filament. In this paper we take closer insight to the effects in modeling of the process with classical cooling by room temperature cross-blow of air below the spinneret outlet. Impact of heating zone we will discuss in a separate paper.

We analyze the sources of the maximum on the take-up velocity *vs.* initial tension plots. Loss of monotonicity of the characteristics, which accompanies stress-induced crystallization at higher take-up speeds, introduces bifurcation of the model solution. Understanding of the sources of the model bifurcation is important for the proper modeling and solving the spinning equations. Example computations are performed for PET.

THE MODEL

We consider a single-filament, steady-state model of melt spinning with predetermined temperature and velocity of the cooling air cross-blow in the cooling zone. Thin filament approximation allows us to neglect radial variation of axial velocity and temperature, and to reduce the problem to one dimension — the axial distance z from the spinneret outlet [5]. In standard spinning conditions, radial gradient of axial velocity can be neglected [6, 7]. Radial temperature gradient can be neglected when the filament is very thin or in the models considering the temperature averaged over the filament cross-section [3].

The model considers velocity profiles $V(z)$ as controlled by the local spinning stress, and local polymer viscosity dependent on local temperature and crystallinity of the spun filament. Kinetics of crystallization of the polymer is controlled by local temperature and local tensile stress. The axial profiles of the filament temperature and tensile stress are controlled by the heat and force balance, respectively.

Point-by-point computation of individual dynamic effect is performed along the spinning axis z for velocity, $V(z)$, temperature, $T(z)$, tensile force, $F(z)$, and tensile stress $\Delta p(z)$, simultaneously with online stress-induced crystallization resulting in a crystallinity profile $X(z)$.

Rheology

In the computations performed for PET we assume purely viscous stress in the spinning line, following all engineering models of the process for this polymer. The simplest rheological model of Newtonian viscous fluid with variable local viscosity $\eta(z)$ is used. Axial changes of viscosity are admitted due to thin-filament assumption and neglected radial variation of temperature.

The non-Newtonian behavior of the spun melt is usually neglected because the sensitivity of the viscosity to deformation rate is much smaller than its sensitivity to local spinning line temperature or crystallinity [3]. Applicability of the Newtonian rheological model for melt spinning of PET was demonstrated by Sano [8] and Lin and Hauenstein [9].

Introduction of viscoelasticity to the dynamics of the process modifies the spinning line profiles [10—12]. Viscoelastic treatment should be considered for melt spinning of high molecular weight polyolefines, while spinning of aliphatic polyesters or polyamides can be approximated by a purely viscous models [8, 9, 11].

The axial velocity gradient of a Newtonian fluid in the spinning process is controlled by the local spinning stress $\Delta p(z)$

$$\frac{dV}{dz} = \frac{1}{3\eta(z)}\Delta p(z) \tag{1}$$

where: $\eta(z)$ — *local shear viscosity of the spun fluid.*

The spinning stress is the local tensile force per local filament cross-section which can be expressed by the filament velocity $V(z)$ from the following mass conservation equation

$$\pi R^2(z)\rho(z)V(z) = W = const \tag{2}$$

where: W — *mass output, constant for a steady-state process,* $R(z)$ — *filament radius,* $\rho(z)$ — *local filament density.*

Using Eq. (2), the spinning stress is expressed by tension $F(z)$, and the filament velocity $V(z)$

$$\Delta p(z) = \frac{\rho(z)V(z)F(z)}{W} \tag{3}$$

Axial variation of the polymer viscosity is a function of axially variable filament temperature and degree of crystallinity

$$\eta(z) = \eta[T(z), X(z)] \tag{4}$$

In the absence of crystallinity, $X = 0$, temperature dependence of the melt viscosity can be approximated for PET by the Arrhenius formula with a single, constant activation energy E_a independent on molecular weight [9, 13]

$$\eta_{melt}(T) = C\exp(E_a/kT) \tag{5}$$

where: C — *coefficient depending on the average molecular weight.*

Eq. (5) provides good approximation in the temperature range well above the glass transition point.

An alternative approximation for the temperature dependence of the melt viscosity is provided by the WLF equation, with the glass transition temperature T_g and shear viscosity $\eta_{melt}(T_g)$ at the glass transition temperature as the parameters [14]

$$\eta_{melt}(T) = \eta_{melt}(T_g)\exp\left[-40.16\frac{T(z)-T_g}{51.6+T(z)-T_g}\right] \tag{6}$$

The Arrhenius and WLF approximations are compared in Fig. 1 for PET melt. The WLF formula significantly deviates from the Arrhenius dependence found experimentally for PET at the temperatures below the

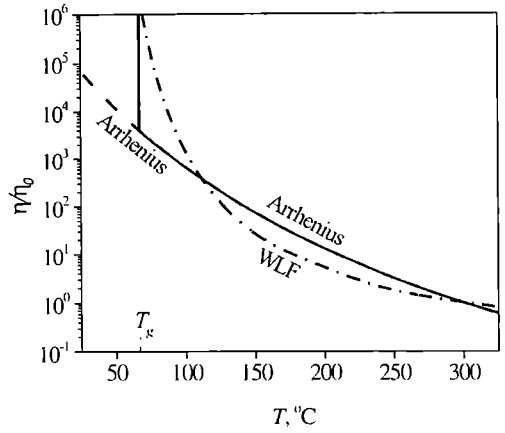

Fig. 1. Reduced shear viscosity (η/η_0) (η_0 — initial viscosity at T_0 = 573 K) vs. temperature (T) predicted by the Arrhenius (dashed line) and WLF (dashed-dotted line) formulae for PET melt. Solid line — approximation used for present computations

melting point. On the other hand, WLF predicts much steeper increase in viscosity near the glass transition point then the Arrhenius formula, less physical in this temperature range.

In the modeling for PET, we adopt the Arrhenius approximation of melt viscosity for the temperatures above T_g as more correct for the spinning range. To account for the steep increase in melt viscosity near the glass transition point, as indicated by WLF formula, we assume infinite viscosity for the temperature range below T_g. The temperature dependence of melt viscosity adopted for computations is given by the solid line in Fig. 1.

Significant effects in polymer viscosity are assigned to crystallinity development, if present. In several mathematical models of melt spinning, rheological effects of crystallinity have been accounted for by introducing polymer viscosity dependent on the degree of crystallinity. Usually, local viscosity $\eta(z)$ of the spun polymer is expressed as a product of temperature dependent local viscosity of non-crystalline melt, $\eta_{melt}(T)$, and a function $\eta_X(X)$ representing effects of crystallization [3, 4, 15, 16]

$$\eta(z) = \eta_{melt}[T(z)]\eta_X[X(z)] \tag{7}$$

In present calculations we assume for the function representing the effect of online crystallization, a formula proposed by Ziabicki [17]. The formula is derived from a general crosslinking theory and it accounts for rheological effects of gelation by crystallization. The crystallites, nucleated and growing in the spun melt, form physical cross-links which interconnect polymer chains.

$$\eta_X(X) = \frac{1}{(1 - X/X^*)^{\alpha}} \tag{8}$$

where: *X^* denotes a critical degree of crystallinity, estimated to be in the range between 0.01 and 0.10, at which gelation by crystallization leads to an infinite network, the exponent α equals unity for low molecular weight and 3.4 for high molecular weight polymer.*

At critical crystallinity, the polymer viscosity shows steep increase to infinity and the polymer solidifies. In present computations, a value of 0.10 is assumed for the critical crystallinity X^*, and unity for the exponent α.

Kinetics of crystallization

Progress in crystallization along the spinning line leads to an axial gradient of the crystallinity degree, dX/dz, which can be expressed by the ratio of local crystallization rate, $\dot{X}$, and local velocity V

$$\frac{dX}{dz} = \frac{\dot{X}}{V} \tag{9}$$

Crystallization of the polymer along the spinning line occurs under non-isothermal conditions and increasing tensile stress. Kinetics of the crystallization is described in a quasi-static approximation by the following Avrami type formula proposed for non-isothermal, stress-induced crystallization [18, 19]

$$\dot{X} = n(1 - X)[-\ln(1 - X)]^{(n-1)/n} \frac{K_{st}(T, \Delta p)}{V} \tag{10}$$

where: *n — Avrami exponent, usually an integer value between unity and four, K_{st} — rate function characterizing the kinetics of steady-state, oriented crystallization at temperature T and tensile stress Δp.*

In this computations we assume the value of Avrami exponent n = 2 determined experimentally by Bragato and Gianotti [20] for crystallization of PET at higher values of the amorphous orientation factor. The authors have found that Avrami exponent reduces from $n \approx 4$ at low amorphous orientation, $f_{am} < 0.13$, to $n \approx 2$ at high orientation, $f_{am} > 0.18$, in preoriented amorphous PET fibers.

The rate function $K_{st}(T, \Delta p)$ has been proposed by Ziabicki [18] and it reads

$$K_{st}(T, \Delta p) = K_{max} \exp\left[-4 \ln 2 \frac{(T - T_{max})^2}{D_{1/2}^2}\right] \exp\left[A f_a^2 (\Delta p)\right] \tag{11}$$

where: *K_{max}, T_{max}, $D_{1/2}$ — maximum value of the rate function, temperature at the maximum, and the function half width at zero tensile stress, respectively; A — oriented crystallization coefficient, a dimensionless empirical parameter which characterizes „effectivity" of the stress in stress-induced crystallization; f_a — amorphous orientation factor controlled by local spinning stress Δp.*

For PET we assume $K_{max} = 0.016\ s^{-1}$, T_{max} = 563 K, and $D_{1/2}$ = 32 deg [21]. Experimental values of the coefficient A, estimated for PET, are in the range 200—1000 [22, 23]. High values of A indicate strong effects of tensile stresses on the kinetics of oriented crystallization.

The amorphous orientation factor f_a increases from zero to unity with increasing in tensile stress from zero

to infinity. Then, f_a should be a non-linear function of the applied stress. The non-linearity should be accounted for in modeling of melt spinning processes which involve high stresses, in particular in high-speed melt spinning.

A correction to the linear stress-orientation law is proposed by a series expansion formula, derived for non-Gaussian chains with inverse Langevin statistics [4, 24]

$$f_a(\Delta p) = \frac{C_{opt}}{\Delta n_a^0}\Delta p - \frac{3}{7}\left(\frac{C_{opt}}{\Delta n_a^0}\Delta p\right)^2 - \frac{1}{7}\left(\frac{C_{opt}}{\Delta n_a^0}\Delta p\right)^3 - \ldots \quad (12)$$

where: C_{opt} — *stress-optical coefficient*, Δn_a^0 — *amorphous birefringence of ideally oriented chains.*

Heat balance

The heat balance equation accounts for the convective heat exchange between the filament and a gaseous surroundings (dry air), and for the heat of crystallization. It yields the following expression for axial gradient of the filament temperature

$$\rho C_p \frac{dT}{dz} = -\frac{2\alpha^*}{RV}(T - T_s) + \rho\Delta h \frac{dX}{dz} \quad (13)$$

where: C_p — *specific heat of the polymer*, α^* — *heat transfer coefficient between the filament and the gaseous surroundings at temperature* T_s, R — *radius of the filament*, Δh — *heat of crystallization per mass unit.*

Heat produced in the bulk by viscous friction is neglected due to thin-filament approximation [3].

The heat transfer coefficient α^* is taken in the form derived by Kase and Matsuo [25, 26] from empirical correlation between the Nusselt and Reynolds numbers

$$\frac{2R\alpha^*}{\lambda_s} = 0.42\left(\frac{2RV}{\nu_s}\right)^{1/3}\left[1 + \left(\frac{8V_y}{V}\right)\right]^{1/6} \quad (14)$$

Local value of α^* is affected by the local filament velocity V and the air cross-blow velocity V_y. It depends also on local filament radius R, as well as on heat conductivity λ_s and kinematic viscosity ν_s of the air. For dry air at room temperature and atmospheric pressure ($\lambda_s = 2.569 \cdot 10^{-4}$ J · cm^{-1} deg^{-1} s^{-1}, $\nu_s = 0.150$ cm^2 s^{-1}), the coefficient reads

$$\alpha^* = 2.034 \cdot 10^{-4}\frac{V^{1/3}}{(2R)^{2/3}}\left[1 + \left(\frac{8V_y}{V}\right)\right]^{1/6} \quad (15)$$

where: α^* *is expressed in* J · cm^{-2} deg^{-1} s^{-1}, R *in cm,* V *and* V_y *in cm* · s^{-1}.

Force balance

The force balance equation accounts for an inertia, air drag, and gravity. It leads to the axial gradient of the tensile force in the following form [3, 10]

$$\frac{dF}{dz} = W\frac{dV}{dz} - \pi R^2\rho g + 2\pi R p_{zr} \quad (16)$$

where: W — *mass output*, g — *acceleration of the gravity*, R — *local radius of the filament*, p_{zr} — *local shear stress at the filament surface resulting from the air friction forces tangential to the spinning axis.*

From the boundary layer theory, the friction stress reads

$$p_{zr} = \frac{1}{2}C_f(R,V)\rho_s V^2 \quad (17)$$

where: ρ_s — *density of the air*, C_f — *empirical coefficient dependent of the filament diameter* R *and velocity* V *[27, 28].*

$$C_f = 0.37\left(\frac{2RV}{\nu_s}\right)^{-0.61} \quad (18)$$

Using $\rho_s = 1.202 \cdot 10^{-3}$ g cm^{-3} and $\nu_s = 0.150 \cdot 10^{-3}$ cm^2 s^{-1} for air at room temperature we have

$$p_{zr} = 6.99 \cdot 10^{-10}\frac{V^{1.39}}{(2R)^{0.61}} \quad (19)$$

where: p_{zr} *is in* $N \cdot cm^{-2}$, R *in cm, and* V *in* $cm \cdot s^{-1}$.

SPINNING EQUATIONS AND THE BOUNDARY CONDITIONS

Single-filament, steady-state melt spinning with on-line stress-induced crystallization is described by the following set of four first-order differential equations for velocity $V(z)$, temperature $T(z)$, crystallinity $X(z)$, and tensile force $F(z)$ profiles

$$\frac{dV}{dz} = \frac{1}{3\eta(T,X)}\frac{\rho FV}{W} \quad (20)$$

$$\frac{dT}{dz} = -0.42\frac{\lambda_s}{C_p}\left(\frac{2}{\nu_s}\right)^{1/3}\left(\frac{\pi}{W}\right)^{5/6}\left(\frac{V}{\rho}\right)^{1/6}\left[1 + \left(\frac{V_y}{V}\right)^2\right]^{1/6}(T - T_s) + \frac{\Delta h}{C_p}\frac{dX}{dz} \quad (21)$$

$$\frac{dX}{dz} = nK_{max}[-\ln(1-X)]^{(n-1)/n}\frac{1-X}{V}\exp\left[-4\ln 2\frac{(T-T_{max})^2}{D_{1/2}^2}\right]\exp\left(\Lambda f_a^2\right) \quad (22)$$

$$\frac{dF}{dz} = W\left(\frac{dV}{dz} - \frac{g}{V}\right) + 0.37\pi\rho_s\left(\frac{2}{\nu_s}\right)^{-0.61}\left(\frac{W}{\pi\rho}\right)^{0.195}V^{1.195} \quad (23)$$

The factor f_a is defined by following equation

$$f_a = \frac{C_{opt}\rho}{\Delta n_a^0 W}VF - \frac{3}{7}\left(\frac{C_{opt}\rho}{\Delta n_a^0 W}\right)^2(VF)^2 - \frac{1}{7}\left(\frac{C_{opt}\rho}{\Delta n_a^0 W}\right)^3(VF)^3 \quad (24)$$

The spinning equations are derived from the rheological equation (1), conservation equations (2), (13), (16), crystallization equations (9), (10), and empirical coefficients given by equations (11), (14), (18).

Steady-state melt spinning requires fixed boundary conditions. In real processes the fixed boundary conditions concern initial velocity, initial temperature, zero crystallinity (pure melt) at the spinneret output, $z = 0$

$$V(z=0)=V_0=\frac{4W}{\pi\rho_0 d_0^2};\quad T(z=0)=T_0;\quad X(z=0)=0 \tag{25}$$

and fixed take-up velocity at the end of the spinning line

$$V(z=L)=V_L \tag{26}$$

where: d_0 — *diameter of the spinneret orifice*, ρ_0 — *initial melt density*.

We do not have any direct control of the tension force F on either boundary. The computational procedure applied for the set of spinning equations (20)—(23) assumes an arbitrary value of the initial tension

$$F(z=0)=F_0 \tag{27}$$

which with the initial conditions, for velocity, temperature and zero crystallinity, equation (25), contributes to the initial value problem. The initial tension force is next adjusted in the procedure to the take-up velocity V_L at the end point.

To solve the spinning equations, temperature of the surrounding air T_s, as well as the air velocity V_y should be specified for the cooling zone. The zone is assumed to be located next to the spinneret output, within the range $0 < z < z_1$, and it is followed by the zone with quiescent air for $z_1 < z < L$. Room temperature of the air is assumed in both zones:

$$\begin{aligned} &0<z<z_1,\quad T_s=293\ \mathrm{K},\quad V_y\neq 0\\ &z_1<z<L,\quad T_s=293\ \mathrm{K},\quad V_y=0 \end{aligned} \tag{28}$$

For dry air at atmospheric pressure we have

$$\rho_{sk}(T_{sk})=\frac{0.35232}{T_{sk}}\quad (\mathrm{g\,cm^{-3}}) \tag{29}$$

$$\lambda_{sk}(T_{sk})=2.0852\cdot 10^{-5}\frac{T_{sk}^{3/2}}{T_{sk}+114}\quad \left(\mathrm{J\,cm^{-1}\,s^{-1}\,deg^{-1}}\right) \tag{30}$$

$$\nu_{sk}(T_{sk})=4.1618\cdot 10^{-5}\frac{T_{sk}^{5/2}}{T_{sk}+114}\quad \left(\mathrm{cm^2\,s^{-1}}\right) \tag{31}$$

Equations (20)—(23) with the initial conditions given by equations (25), (27) and zone conditions given by equation (28) provide an initial value problem which can be solved by step-by-step computations along the spinning axis z.

We assume local density ρ and specific heat C_p of the polymer dependent on local temperature

$$\rho(z)=\rho_0-\rho_1[T(z)-273] \tag{32}$$

$$C_p(z)=C_{p0}+C_{p1}[T(z)-273] \tag{33}$$

where: ρ_0, ρ_1, C_{p0}, C_{p1}, *are material constants*.

SIMPLIFIED DYNAMIC EQUATIONS

Closed analytical solution of the melt spinning equations can be obtained for some simplified cases with the air drag and gravity forces neglected. We consider two simplified cases leading to the analytical solution of the dynamic equation (23). The simplest one is the case with neglected inertia force, in addition to neglected air drag and gravity, and the second one with the inertia force accounted for. When the inertia force is neglected together with air drag and gravity forces, the axial gradient of the spinning line tension is zero and equation (23) reduces to

$$\frac{dF}{dz}=0 \tag{34}$$

The second case accounts for inertia force alone, at neglected air drag and gravity forces, and the dynamic equation (23) reduces to

$$\frac{dF}{dz}=W\frac{dV}{dz} \tag{35}$$

In the first case, without the inertia force, a constant tension along the entire spinning line is obtained

$$F(z)=F_0 \tag{36}$$

Then equation (20) for the velocity gradient simplifies to

$$\frac{dV}{dz}=\frac{\rho(z)}{3\eta(z)W}F_0V \tag{37}$$

and axial profile of the filament velocity for initial velocity V_0 reads

$$V(z)=V_0\exp\left[\frac{F_0}{3W}\int_0^z\frac{\rho(z)dz}{\eta(z)}\right] \tag{38}$$

From the above equation we obtain the following relation between the initial force F_0 and the final take-up velocity V_L

$$V_L=V(z=L)=V_0\exp\left(\frac{\rho_0F_0I_L}{3W}\right) \tag{39}$$

I_L is defined by

$$I_L=\int_0^L\frac{\rho(z)}{\rho_0}\frac{dz}{\eta(z)} \tag{40}$$

where: ρ_0 — *melt density at the spinneret output*, $z = 0$.

The integral I_L is controlled by the axial profile of the polymer viscosity $\eta[T(z), X(z)]$, strongly affected by the profiles of temperature and degree of crystallinity. Changes in the viscosity due to changes in temperature and crystallinity along the spinning line dominate by orders of magnitude changes in density, $\rho(z)$. Then, assuming $\rho(z)/\rho_0 = 1$ for equation (40), I_L can be very well, approximated by the integral of the inverse viscosity between $z = 0$ and the final point $z = L$

$$I_L=\int_0^L\frac{dz}{\eta(z)} \tag{41}$$

which characterizes fluidity of the polymer within the entire spinning line.

In the case with inertia force accounted for, integration of the dynamic equation (35) with the initial condition given by equation (27) leads to the following relation between local tension $F(z)$ and velocity $V(z)$

$$F(z) = F_0 + W[V(z) - V_0] \tag{42}$$

Then equation (20) for the velocity gradient reads

$$\frac{dV}{dz} = \frac{\rho(z)}{3\eta(z)W}[F_0 + W(V - V_0)]V \tag{43}$$

and its integration with the initial velocity V_0 leads to the following expression of the velocity profile

$$V(z) = V_0 \frac{F_0 - WV_0}{F_0 \exp\left[-\frac{F_0 - WV_0}{3W}\int_0^z \frac{\rho(z)}{\eta(z)}dz\right] - WV_0} \tag{44}$$

The relation between final velocity V_L and the initial force F_0 reads then

$$V_L = V_0 \frac{F_0 - WV_0}{F_0 \exp\left[-\frac{\rho_0(F_0 - WV_0)I_L}{3W}\right] - WV_0} \tag{45}$$

where the effects of viscosity are also represented by the integral I_L, similarly like in the case without the inertia force. When the product WV_0 in equations (44) and (45) is replaced by zero, then they reduce to equations (38) and (39) derived for the model without inertia.

In both cases, without and with inertia, axial velocity profiles $V(z)$ are controlled by the integral of inverse viscosity between the initial point $z = 0$ and the current point z. The integral represents fluidity of the polymer in that part of the spun filament.

Equations (39) and (45) indicate, that the relation between final take-up velocity V_L and the initial force F_0 is controlled by the integral fluidity of the polymer, I_L, within the entire spinning line. Value of the integral is limited by the ratio of the position of the solidification point z_{sol} to the initial melt viscosity ratio η_0

$$I_L = \frac{z_{sol}}{\eta_0}\int_0^1 \frac{dx}{\eta(x)/\eta_0} < \frac{z_{sol}}{\eta_0} \tag{46}$$

where: *the variable* $x = z/z_{sol}$.

Equation (46) is obtained from equation (40) assuming infinite viscosity of the polymer in the filament below the solidification point, $z > z_{sol}$. The inequality appears because viscosity of the polymer at any point of the spinning line exceeds the initial viscosity, $\eta(x) > \eta_0$.

RESULTS AND DISCUSSION

Relations between take-up velocity V_L and the initial force F_0 obtained from the simplified dynamic models are used to discuss an impact of spinning conditions on the filament rheology and spinning dynamics. This concerns in particular high take-up speeds which may lead to online stress-induced crystallization of the polymer.

Figures 2 and 3 illustrate V_L *vs.* F_0 plots computed from equations (39) and (45) for the models without and with the inertia force, respectively. Shapes of the plots are sensitive to the character of the dependence of the

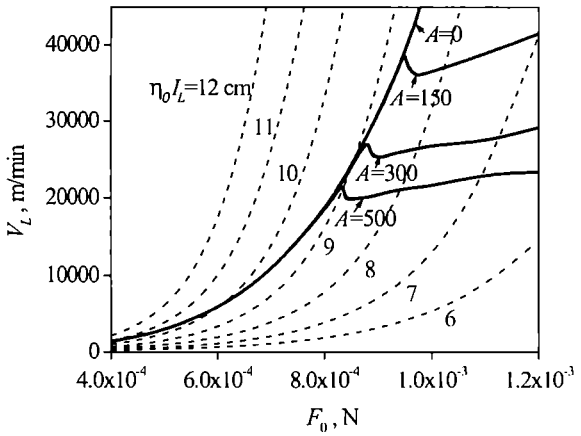

Fig. 2. Take-up velocity (V_L) vs. initial force (F_0) predicted for PET from the simplified model without an inertia; solid lines — computed for I_L dependent on F_0 at different values of A, dashed lines — computed with the assumption I_L = const. η_0 — initial viscosity at T_0 = 573 K

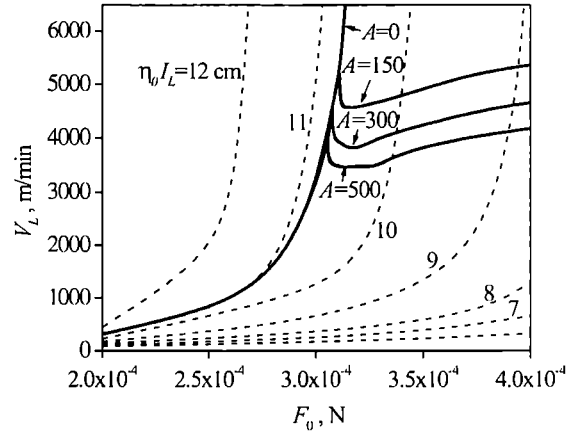

Fig. 3. Take-up velocity (V_L) vs. initial force (F_0) predicted for PET from the simplified model without an inertia. Lines — like in Figure 2

integral I_L on the F_0. If we assume that the integral I_L is fixed, independent on F_0, then V_L increases monotonically to infinity with increasing F_0, as illustrated in Figures 2 and 3 by the dashed lines computed for different values of I_L. The assumption of fixed I_L, independent on F_0, is unphysical for processes involving stress-induced crystallization where an increase in the initial force introduces fast oriented crystallization which strongly affects the viscosity profile [$\eta(z)$]. Local temperature and local degree of crystallinity of the polymer are determined from the equations (21) and (22), considering appropriate cooling conditions specified for the process.

We will discuss the effects of the viscosity profile on two processes which differ in temperature treatment along the spun filament. The first one, with online cooling in the vicinity of the spinneret outflow is discussed below in this paper. The second one with online zone heating by a high-temperature chamber with hot air positioned next to the cooling zone, and before the take-up point, will be discussed in a separate publication.

Here we consider the melt spinning with cooling by the air cross-blow within a limited zone, located next to the spinneret, using both simplified models without and with an inertia, as well as full dynamic model represented by equations (20)—(23) with appropriate boundary conditions. The computations are performed for PET assuming initial melt temperature T_0 = 573 K, intrinsic viscosity of the polymer [η] = 0.6, diameter of the spinneret orifice d_0 = 0.03 cm, and fixed mass output with the value W = 0.04 g/s for each process. Cross-blow velocity of the cooling air V_y = 40 m/s, and temperature of the air T_s = 293 K are taken. The same temperature of air is assumed for the zone which follows the zone with the air cross-blow. Length of the zone with the air cross-blow is assumed to be 100 cm, and length of the entire spinning line L = 300 cm.

The computations indicate that the fluidity integral I_L is significantly affected by the initial force, and it cannot be assumed as independent on F_0. The plots in Figures 4 and 5 illustrate I_L *vs.* F_0 relations computed for both simplified models using equations (21) and (22) at different values of the oriented crystallization coefficient A = 0, 150, 300 and 500. Step-by-step computations of the temperature and crystallinity profiles have been performed. Values of I_L in the figures are reduced by the initial melt fluidity at the spinneret output, $1/\eta_0$.

The plots in Figures 4 and 5 show that the integral I_L decreases with increasing F_0. In the range of small values of F_0 the decrease is rather moderate and results from more intensive cooling at faster flow of the polymer at higher tensions. At a critical value of F_0, sharp transition to much steeper relation, with more negative slope, is predicted. The transition is not seen at A = 0, at which oriented crystallization is switched off, and it appears at high enough values of the coefficient A. We find that the value of A should be above 100 to have such transition, and the transition shifts to lower values of F_0 with increasing A.

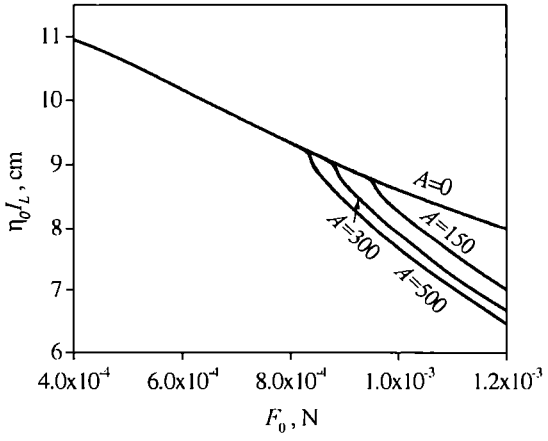

Fig. 4. Reduced fluidity integral ($\eta_0 I_L$) vs. initial force (F_0) computed for PET from the simplified model without an inertia at different values of A

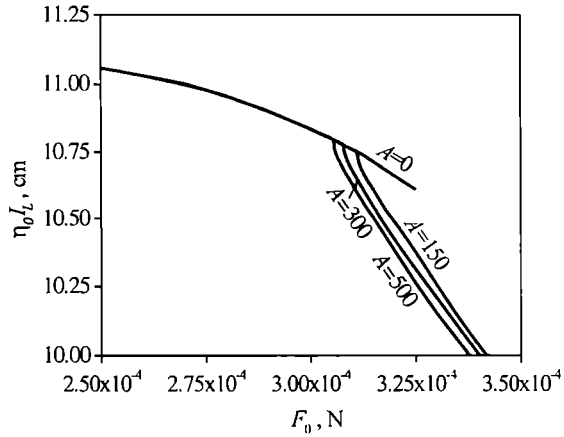

Fig. 5. Reduced fluidity integral ($\eta_0 I_L$) vs. initial force (F_0) computed for PET from the simplified model with an inertia at different values of A

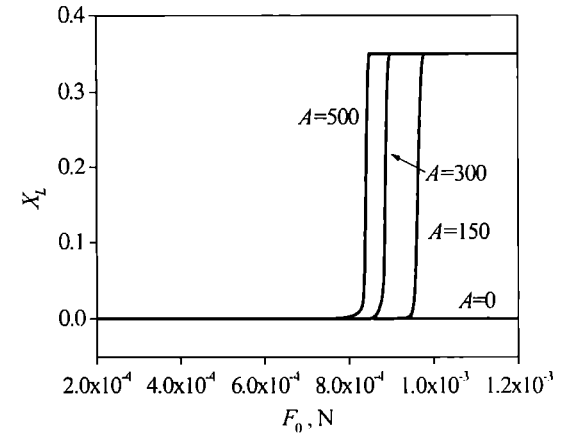

Fig. 6. Crystallinity (X_L) of as-spun fiber vs. initial force (F_0) computed for PET using simplified dynamic model without an inertia at different values of A

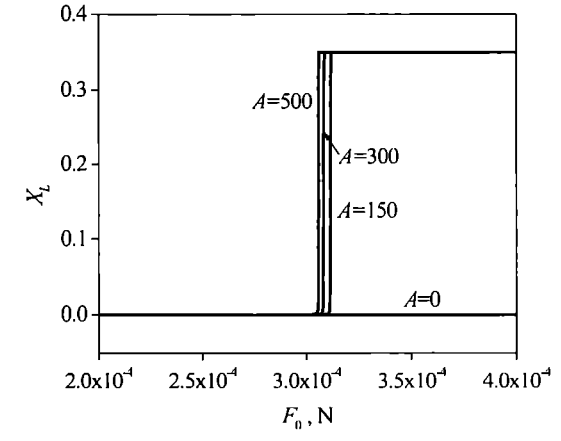

Fig. 7. Crystallinity (X_L) of as-spun fiber vs. initial force (F_0) computed for PET using simplified dynamic model with an inertia at different values of A

Figures 6 and 7 show final degree of crystallinity X_L of the filament at the take-up point *vs.* initial tension F_0, computed for the simplified models without and with an

inertia, respectively. Final degree of crystallinity, achievable in the process, is limited in our computations to the value of 0.35. We find that the sharp transitions of the I_L *vs.* F_0 plots to much more negative slope, as illustrated in Figures 4 and 5, coincide with an onset of oriented crystallization of the polymer at a critical value of F_0.

Cause of the sudden change to much more negative slope of the I_L *vs.* F_0 relation should be assigned to oriented crystallization, induced in the processes with initial force exceeding the critical value. This indirect effect of initial force on the integral fluidity I_L, *via* oriented crystallization, has significant impact on the spinning process and its dynamics.

A consequence of the online stress-induced crystallization and its effects on polymer viscosity is an appearance of a maximum of the relationship between V_L and F_0. Such a maximum is predicted by both analytical formulae, equations (39) and (45), derived for take-up velocity V_L from the simplified dynamic models. We find using these models that V_L is a function of the initial force F_0 and fluidity integral I_L which is a function of F_0

$$V_L = V_L[F_0, I_L(F_0)] \tag{47}$$

The necessary condition for the maximum of V_L reads

$$\frac{dV_L}{dF_0} = -\frac{\partial V_L}{\partial F_0} + \frac{\partial V_L}{\partial I_L}\frac{dI_L}{dF_0} = 0 \tag{48}$$

The maximum appears when variation of the fluidity integral I_L, with increasing F_0, satisfies the relation

$$\frac{dI_L}{dF_0} = -\frac{\partial V_L}{\partial F_0} \Big/ \frac{\partial V_L}{\partial I_L} \tag{49}$$

Equations (39) and (45) indicate that partial derivatives in equation (49) are positive, $\partial V_L / \partial F_0 > 0$ and $\partial V_L / \partial L_L > 0$. Then, in consequence, the derivative dI_L/dF_0 should be negative at the maximum, and high enough to compensate an increase in take-up velocity with increasing F_0 at fixed value of I_L. Realization of such strong condition is provided by oriented crystallization induced in the filament at high initial force which strongly affects slope of the I_L *vs.* F_0 relationship, as illustrated in Figs. 4 and 5.

The V_L *vs.* F_0 plots computed from the simplified models, equations (39) and (45), using integral fluidity I_L affected by F_0 (due to stress-induced crystallization and cooling) are shown in Figures 2 and 3 by the solid-line plots. The plots illustrate that strong reduction in the fluidity integral I_L, caused by stress-induced crystallization, disturbs monotonic character of the characteristics and leads to a maximum. The plots are calculated at different values of oriented crystallization coefficient A.

The maximum of V_L appears in both models, without and with an inertia, but at different initial forces. In the case of the model without an inertia, the maximum values of take-up velocity and initial forces corresponding to the maximum are much higher than in the case of more realistic model with an inertia. Nevertheless, maximum of take-up velocity appears in both dynamic models, and its value is the lower, the higher is the value of A.

In the case of no oriented crystallization, $A = 0$, the V_L *vs.* F_0 plots in the Figures 2 and 3 remain monotonic. They does not show any maximum, although they deviate from steep dashed-line plots computed for fixed values of I_L. The $A = 0$ plots correspond to a process without stress-induced crystallization, and illustrate the effects of viscosity resulting from the cooling itself. One concludes that the effects of cooling, isolated from the effects of oriented crystallization, are not strong enough to disturb monotonicity of the V_L *vs.* F_0 plots and introduce a maximum. The $A = 0$ plots in Figures 2 and 3 traverse nevertheless the dashed-line plots predicted for fixed values of I_L,, from higher to lower, with increasing F_0 as the consequence of cooling.

The refinement of individual effects in the dynamic of melt spinning, performed for the simplified models, indicates that the maximum of the take-up speed V_L *vs.* F_0 is a consequence of strong effects of oriented crystallization in the polymer viscosity. Our computations indicate that the maximum of V_L corresponds to the spinning process producing filaments with final degree of crystallinity of about 1—2 % at the take-up point. The effects discussed are not related to the heat of crystallization, which contributes rather to an enhancement of the polymer fluidity, but to cross-linking of the chain macromolecules by the crystallites in early stages of crystallization.

The complete dynamic model of melt spinning with online oriented crystallization, equations (20)—(23), also predicts the maximum of the V_L *vs.* F_0 plots, as shown in Figure 8 for different values of the oriented crystallization coefficient A between zero and 500. The plots resemble those predicted from the simplified model with

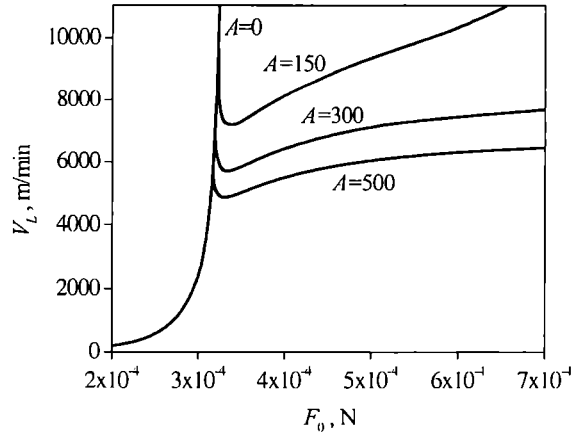

Fig. 8. Take-up velocity (V_L) vs. initial force (F_0) computed for PET from the complete dynamic model at different values of A

the inertia force accounted for, shown in Figs. 2 and 3 by the solid lines. Positions of the maximum for each A in both models, with an inertia and the complete one, are very close. Values of the take-up velocity at the maximum predicted in the complete dynamic model are higher. The discrepancy in the maximum values is related to the air drag forces, not accounted for in the simplified model, which induce oriented crystallization at higher take-up speeds in the case of complete model.

The plots in Fig. 8 indicate again that stress-induced crystallization introduces limitation of the take-up velocity. The maximum value of V_L depends on sensitivity of the kinetics of oriented crystallization on the applied stresses, represented by the coefficient A. The higher is the coefficient, the lower is the maximum value of V_L.

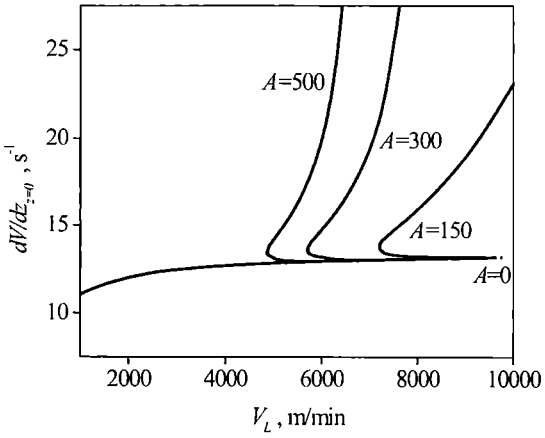

Fig. 9. Initial velocity gradient $[(dV/dz)_{z=0}]$ vs. take-up velocity (V_L) computed for PET from the complete dynamic model at different values of A

Figure 9 shows the plots of the initial velocity gradient at the spinneret output $[(dV/dz)_{z=0}]$ *vs.* take-up speed V_L computed for different values of A. The initial velocity gradient is determined from the initial force

$$\left(\frac{dV}{dz}\right)_{z=0} = \frac{4F_0}{3\pi d_0^2 \eta_0} \tag{50}$$

The plots show bifurcation of the initial gradient of velocity at higher values of the take-up velocity at which stress-induced crystallization takes place. The bifurcation appears at lower take-up speeds for higher values of the coefficient A. The lower velocity gradients in the bifurcation lead to amorphous fibers, while the higher once result in crystalline fibers. The bifurcation predicted in the model is a consequence of strong increase in polymer viscosity due to stress-induced crystallization and gelation of the structure by crystalline crosslinking.

ACKNOWLEDGEMENT

This paper resulted from the research supported by Research Grant PB 7 T08E 026 18 from the Polish State Committee for Scientific Research (KBN).

REFERENCES

1. U.S. Pat. 4 134 882 (1979).
2. „High-Speed Melt Spinning" (Eds. Ziabicki A., Kawai H.), Wiley, New York 1985.
3. Ziabicki A., Jarecki L., Wasiak A.: *Comput. Theoret. Polym. Sci.* 1998, **8**, 143.
4. Jarecki L., Ziabicki A., Blim A.: *Comput. Theoret. Polym. Sci.* 2000, **10**, 63.
5. Petrie C. J. S.: „Elongational Flow", Pitman, London 1979.
6. Ziabicki A.: *Kolloid Z.* 1961, **175**, 1961.
7. Kase S. J.: *Appl. Polym. Sci.* 1974, **18**, 3267.
8. Sano Y., Orii K., Yamada N.: *Sen-I Gakkaishi* 1968, **24**, 147.
9. Lin L. C. T., Hauenstein J.: *J. Appl. Polym. Sci.* 1974, **18**, 3509.
10. Ziabicki A.: „Fundamentals of Fiber Formation", Wiley, London 1976, p. 63.
11. Chen Z., Papanastasiou A. C.: *Int. Polym. Proc.* 1987, **2**, 33.
12. Mitsoulis E., Beaulne M.: *Adv. Polym. Technol.* 2000, **19**, 155.
13. Dutta A., Nadkarni V. M.: *Textile Res. J.* 1984, **54**, 35.
14. Williams M. L., Landel R. F., Ferry J. D.: *Am. Chem. Soc.* 1955, **77**, 3701.
15. Shimizu J., Okui N., Kikutani T. in: „High Speed Fiber Spinning" (Eds. Ziabicki A., Kawai H.), Wiley, New York 1985, p. 173.
16. Katayama K., Yoon M. G. in: [15], p. 207.
17. Ziabicki A.: *J. Non-Newtonian Fluid Mech.* 1988, **30**, 157.
18. Ziabicki A.: *Colloid Polym. Sci.* 1974, **252**, 207.
19. Ziabicki A.: *Colloid Polym. Sci.* 1996, **274**, 209.
20. Bragato G., Gianotti G.: *European Polym. J.* 1983, **19**, 803.
21. Ziabicki A.: in [10], p. 113.
22. Wasiak A.: Reports of Institute Fundamental Technol. Res., Warsaw 1973, No 39.
23. Alfonso G. C., Verdona M. P., Wasiak A.: *Polymer* 1978, **19**, 711.
24. Ziabicki A., Jarecki L.: *Colloid Polym. Sci.* 1986, **264**, 343.
25. Kase S., Matsuo T.: *J. Polymer Sci.* 1965, **A-3**, 2541.
26. Kase S., Matsuo T.: *J. Appl. Polym. Sci.* 1967, **11**, 251.
27. Matsui M.: *Trans. Soc. Rheol.* 1976, **20**, 465.
28. Gould J., Smith F. S.: *J. Textile Inst.* 1980, **71**, 38.

Received 7 IV 2003.